A Technique for Testing Airfoil Sections at Transonic Speeds

RICHARD E. WALLACE* AND JOHN R. MONK†
The Boeing Company, Renton, Wash.

Transonic airfoil sections have received renewed interest as the result of recently developed design techniques. This caused the need for a simple, versatile, and more rapid method of evaluating airfoils in the wind tunnel. Airfoil test techniques in the Boeing Transonic Wind Tunnel were required to have minimum departure from the normal tunnel configurations. The wing models were mounted vertically from the solid-floor turntable with a test region contained between two large horizontal end plates. This technique produced accurate data at a section Reynolds number of approximately 6,000,000. An on-line analog system provided plots of the section pressure distributions, wake profiles, and drag polars for immediate analysis. Also, flow-field static pressures, shadowgraph pictures, and boundary-layer surveys were obtained.

Nomenclature

C_{AP}	=	axial force coefficient from integrated pressures
C_D	=	section drag coefficient
C_L	=	section lift coefficient
C_{NP}	=	normal force coefficient from integrated pressures
C_P	=	section pressure coefficient
C_{P^*}	=	sonic pressure coefficient
K	=	angle-of-attack factor to correct for model finite span
M	=	freestream Mach number
M_{DD}	=	drag divergence Mach number, $dC_D/dM = 0.1$
P_S	=	freestream static pressure
P_{SWR}	=	wake-rake static pressure
P_T	=	freestream total pressure
P_{TWR}	=	wake-rake total pressure
Q	=	wind-tunnel dynamic pressure, psi
R_N	=	normal-flow Reynolds number
X/C	=	normalized chordwise coordinate
Y/C	=	normalized vertical coordinate
α	=	corrected angle of attack, deg
α_G	=	geometric test angle of attack, deg
$\delta P_T/Q$	=	normalized total-pressure differential
η	=	model span fraction

Introduction

THE Boeing Company became interested in transonic airfoil testing over 20 yr ago when airfoil sections were being designed for application to the B-47. The goal of this experimental work was to extend the NACA low-drag airfoil information by combining thickness and camber distributions to produce improved aerodynamic performance with geometries suitable for aircraft production. As a result, airfoil sections were generated with structurally feasible shapes that avoided concave surfaces. These successful experiments also served as the basis for the wing designs of the B-52 and the 707 and 727 commercial transports.

The wind-tunnel apparatus used for these experiments is illustrated in Fig. 1. All of the data were obtained by pressure instrumentation on 6-in. chord models that spanned the 1-ft gap between two airfoil-sectioned walls. Standard manometer practice was used for the wake surveys and for the surface pressures obtained with freestream Mach numbers to 0.9 and lift coefficients to 1.0. The envelope of drag divergences of these airfoils is shown in Fig. 2 as 1945 technology. This airfoil operating regime was typical for airplanes of the early jet era. It was against this background of successful airfoil development that the new methods of design and testing were required to show an improvement.

Received December 9, 1964; revision received August 16, 1965.

* Senior Group Engineer for Transonic and Supersonic Aerodynamic Research, Airplane Division. AIAA Member.

† Aerodynamicist, Aerodynamics Staff, Airplane Division. AIAA Member.

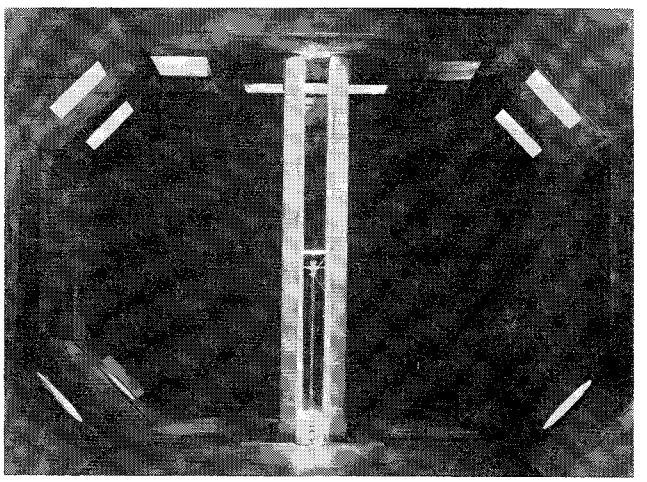

Fig. 1 Transonic airfoil test apparatus of 1945.

Reasons for Renewed Interest in Transonic Airfoils

A major reason for renewed interest in transonic airfoils is the advent of aircraft designed to cruise at supersonic speeds. The very high sweep angles necessary for efficient flight at supersonic speeds require significantly higher section lift coefficients than are necessary for subsonic jets. Also, supersonic airplanes operate at high section Reynolds' numbers, which, as indicated in Fig. 3, can give significantly higher lift if taken into account in the design. This consideration be-

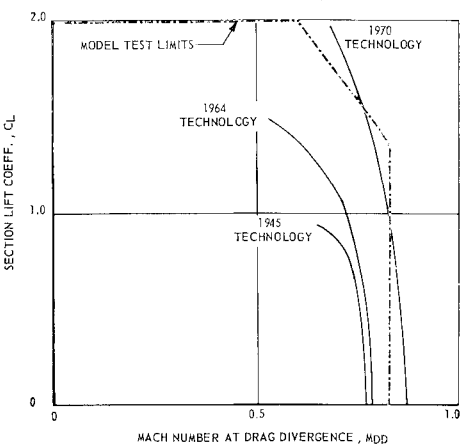

Fig. 2 Regions of interest.

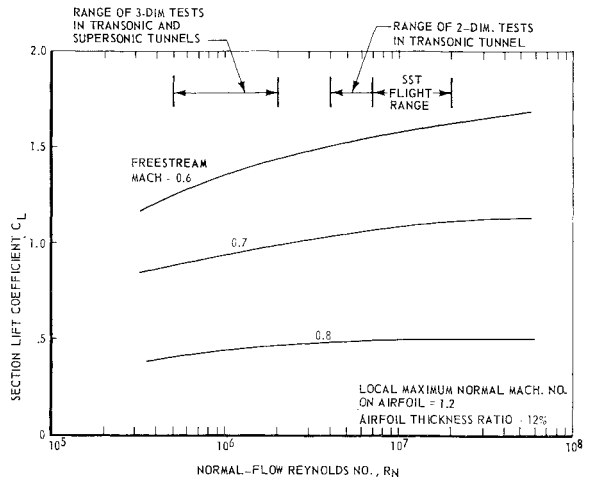

Fig. 3 Typical viscous limitations on design lift.

comes less important as the freestream normal Mach number is increased, which is shown by this figure.

Advances in the empirical and theoretical methods of transonic airfoil design have occurred for several reasons. Extensive flight experience, with wings having transonic flow over their upper surface during cruise, has shown that the turbulent boundary layer can withstand, without separation, the pressure gradients imposed by moderate shock waves. Hence, airfoils can operate efficiently with extensive regions of supersonic flow on them, even when this region is terminated by a shock system. This has resulted in the generation of new design concepts for airfoils.[1,2] Recent studies of the turbulent boundary layer provide significant improvements in the theoretical understanding of growth rate and separation characteristics, and procedures for optimizing pressure distributions governed by boundary-layer criteria have been illustrated in principle.[3,4] Another objective of the test method described in this paper was to evaluate complex theories that predict a shock-free supersonic zone such as that illustrated in Fig. 4.

When renewed transonic airfoil development was initiated, the following test requirements were established: 1) Reynolds number should be as high as practical, 2) side wall boundary layer should be minimum, 3) transonic pressure relief should be provided by the existing slotted-wall configuration, 4) there should be minimum conversion complexity from the normal test section configuration, 5) models should be large for good dimensional accuracy, 6) test data should be accurate and repeatable, and 7) latest instrumentation techniques should be utilized.

Test Technique Adopted

The installation developed for transonic airfoil testing in the Boeing Transonic Wind Tunnel is illustrated in Fig. 5. The wing sections and the wake rake are cantilevered from the unslotted-floor turntable. The wake rake can be moved normal to the model chord plane and rotated, in addition to the turntable motion that maintains approximately correct rake position. The rake is aligned by remote control to correspond to the location and direction of the wake flow. Flow angularity is indicated by a yaw head on the wake rake.

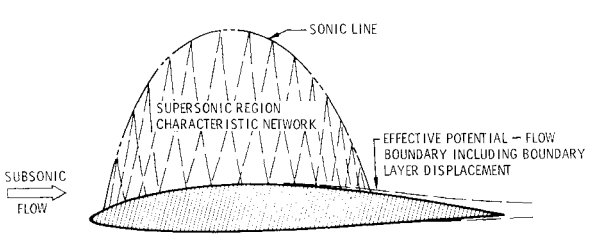

Fig. 4 Transonic airfoil section with idealized flows.

Figure 5 shows the window in the upper end plate and the mirror in the lower end plate used for the double-pass shadowgraph system. In later tests, pressure taps were eliminated from the mirror for image clarity. End plate segments containing pressure orifices or the shadowgraph mirror can be interchanged in a segment of the lower end plate that is stabilized by the strut shown in Fig. 5.

The size of the end plates was chosen to give a local lift loading within $\pm 2\%$ of the mean value. This particular geometry gives the test section a lift-curve slope equivalent to an aspect-ratio seven wing, where the lower end plate serves primarily as a floor boundary-layer splitter. The span loading diagram and the aspect-ratio correction on angle of attack are shown by Figs. 6a and 6b, respectively.

Static pressure distribution of the wing section is measured with orifices located midway between the two end plates (Fig. 7). Additional static pressure orifices located on the lower end plate determine the pressures in the transonic flowfield above the airfoil. These orifices can be seen in the mirror of Fig. 5 and as sketched in Fig. 7. The various orifices and the wake rake are connected to pressure transducers by means of scanning valves. Figure 7 also shows the trip strip, which consists of individual center-punch craters located at 10% chord on 0.4-in. centers with a mean lip height of 0.0022 in. on a 20-in.-chord model.

Figure 8 is a schematic representation of the data system and the data plots produced by it. The system has two branches. One gives on-line data for monitoring the test, and the other records more accurate digital data for later processing. These branches are indicated by the open and solid arrows, respectively, with the common elements crosshatched. In both cases the lift and drag are obtained by integration of the surface and the wake-rake pressures. A novel feature of the digital system is interpolation of the end plate data to give flow-field isobars from the electronic plotter.

Typical final data plots of wing pressure distributions and wake profiles made by the electronic plotter[5] are shown in Figs. 9a and 9b. These plots are produced on a General Dynamics SC 4020 machine that uses a digitally controlled cathode-ray tube trace to expose a 35-mm film, which serves as final data

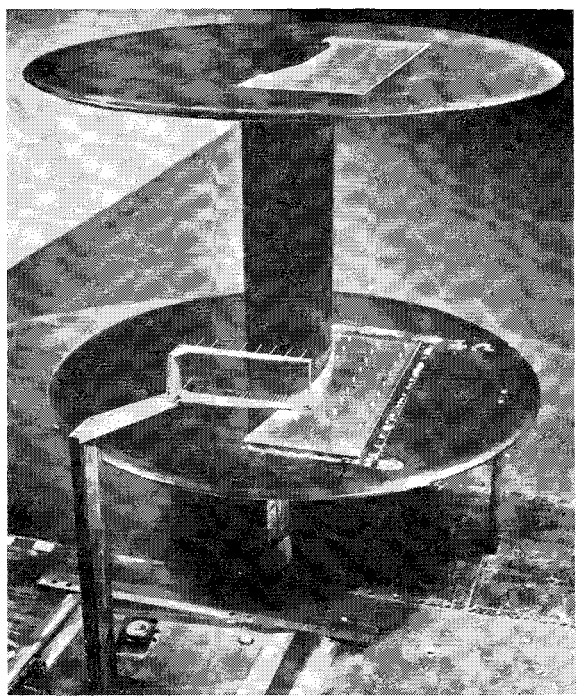

Fig. 5 Transonic airfoil test installation in 8- × 12-ft tunnel.

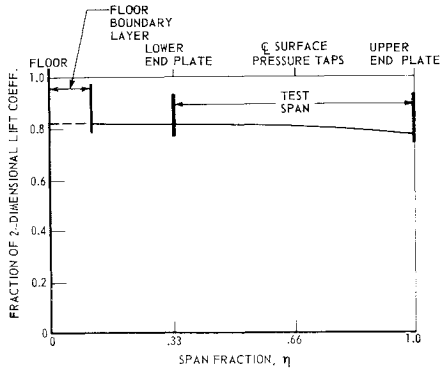

Fig. 6a Theoretical lift distribution.

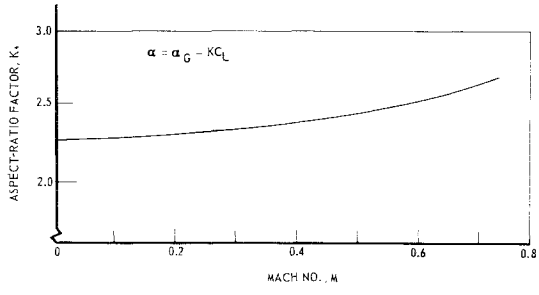

Fig. 6b Theoretical angle-of-attack correction.

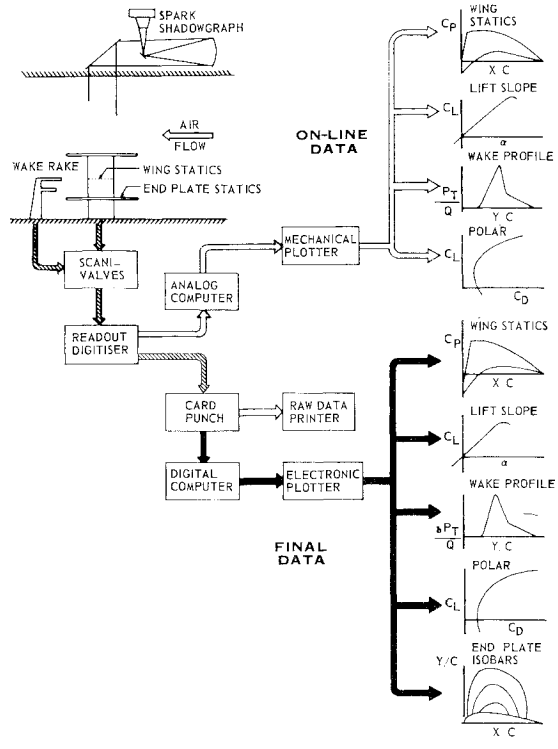

Fig. 8 Data system schematic.

storage and vellum copy source. This data system makes the final aerodynamic data available overnight. A two-shift test period, which is generally devoted to investigating a given airfoil, produces about 150 individual plots of the types shown.

Sufficient angle-of-attack and Mach number combinations are run to give good definition of the drag divergence boundary throughout the airfoil lift range. It has been possible to obtain good data into the buffet region of the airfoil, although when the shock wave gets extensive in height, double positioning of the wake rake becomes necessary for accurate drag measurements.

A schematic of the double-pass shadowgraph is shown in Fig. 10. The double-pass light path was required by the cantilevered model installation, which permitted access from only one end. A single-pass system was attempted earlier by photographing the shadow image cast on the lower end plate, but the shadow resolution and oblique angle of the picture made this approach unsatisfactory.

Additional constraints on the shadowgraph system were the transonic slots in the tunnel ceiling. This forced the system off-center laterally to a window located between slots and restricted the window width (or the picture height) to 8 in.

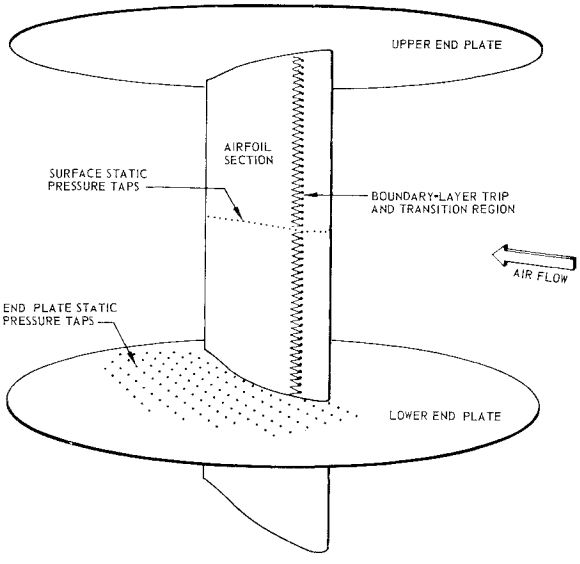

Fig. 7 Typical model details.

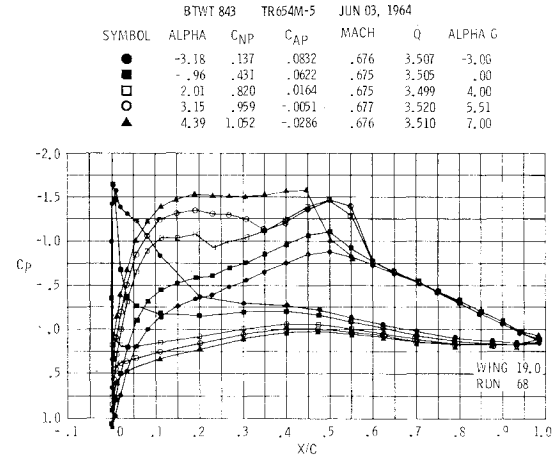

Fig. 9a Electronically plotted section pressure distributions.

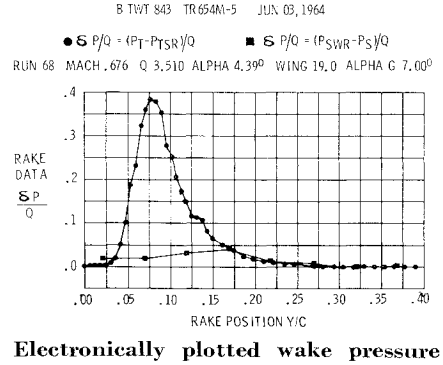

Fig. 9b Electronically plotted wake pressure profiles.

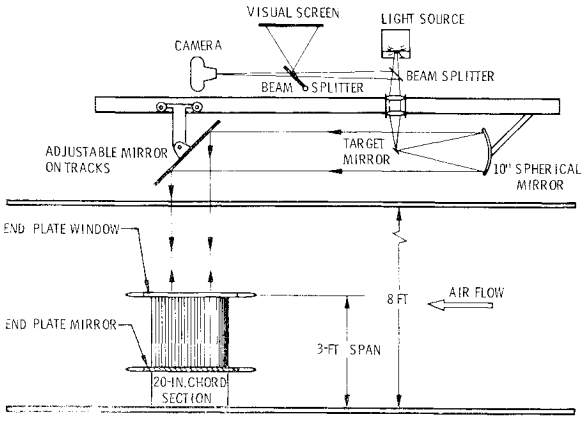

Fig. 10 Double-pass shadowgraph schematic.

The spherical mirror limits the chordwise field coverage to 10 in., so that two pictures are required to cover the boundary-layer development and the downstream part of the sonic region as shown by Figs. 11a and 11b. The dark shadow of the target mirror in these photographs was eliminated subsequently by off-setting the light system to hide the shadow behind the model.

The photographs of Figs. 11a and b show typical flow conditions above and below drag divergence that result from shock interaction with the boundary layer. Sonic lines are sketched onto these figures to illustrate the supersonic-flow-region correlation available from pressure orifices in the interchangeable end plates. It is fairly typical of conditions in the drag divergence regime that strong interaction occurs between the shock waves and the sidewall boundary layers, so that the end plate pressure data are used primarily below the drag divergence. The poor correspondence in Fig. 11b between the shock position and the end plate sonic region is the result of such sidewall boundary-layer interference.

Two types of boundary-layer surveying devices are used to measure the boundary-layer development over airfoil surfaces. A single fine probe is used to measure thin boundary layers on the forward part of the airfoil, whereas a rake is used to measure boundary layers near the trailing edge of the airfoil where the boundary layer is significantly thicker. These measuring devices, in conjunction with the wake rake, are used to investigate the complete history of the boundary layer through those conditions (angle of attack and Mach number combinations) that lead to separation. These data are obtained on repeat runs chosen to provide correlations between the momentum and displacement thickness distributions measured and those computed from the corresponding pressure distributions. Surveys are taken off-center from the model test section to minimize the interference of the centerline array of pressure taps with the boundary layer being measured.

Evaluation of Technique

One of the methods used to determine the adequacy of this test method was to compare data on an NACA thickness distribution airfoil with similar data from NACA facilities. A symmetrical section was tested to establish a zero-camber performance reference for other work which also then served as an evaluation section. Results of comparing this NACA 65-010.4 section data with NACA 64-010 64A010, and 64A012 data from Langley and Ames tunnels[6,7] are shown as Figs. 12a and 12b.

Figure 12a compares drag divergence Mach boundaries for the sections that all have zero camber but differing thickness distributions. Drag divergence for this comparison has been defined as dC_D/dM of 0.1. The NACA tests were made at a Reynolds number of 1,000,000, whereas the Boeing tests were at 5,500,000. This test condition difference could influence the shock-induced boundary-layer separation to occur sooner in the NACA tests. It is striking to note that the 10% sections had a lower drag-divergence Mach boundary than the 12% section tested in a different NACA facility.

The Boeing tests of the 10.4%-thick section showed somewhat higher Mach number for drag divergence than the thinner NASA section of 10.0% thickness. Since only untripped boundary-layer data were available from NACA tests, the Boeing data also were taken without tripping the boundary layer. It was concluded from these results that reasonably good drag divergence data could be obtained by this test technique, at least within the scatter of other results.

Lift curves and drag polars, shown as Fig. 12b, indicate similar correlation with the NACA data. The NACA 64-010 lift-curve slope is closest to the Boeing test data, whereas the 6A-series 10 and 12% sections have lower slopes with the thicker section being lowest. Drag polars show the most pronounced influence of the higher Reynolds number used in the Boeing 65-010.4 airfoil tests. Not only is there a significant reduction in skin friction, but the drag force break occurs at a slightly higher lift coefficient, which is opposite to the effect normally expected from a more rearward maximum thickness section.

Although these checks against results from other facilities provided reasonable confidence in this test apparatus, it should be borne in mind that usage is primarily for airfoil development. This emphasizes relative airfoil performance more than absolute data or strict correlation with other facilities. Therefore, data reproducibility from one test period, or portion of test, to another is of primary importance. When care has been taken with the model surface finish, trip strip, end plate sealing, etc., the test data have been duplicated quite accurately. This has been determined in several cases where the original data were later extended by more detailed testing.

Another criterion of test technique adequacy is the two-dimensionality of the airfoil flow between the end plates. Figures 13a and 13b show the fairing of end plate isobars to the airfoil surface pressures measured at the center of the

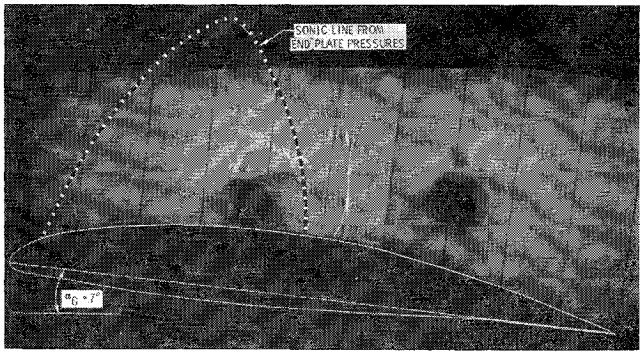

Fig. 11a Spark shadowgraph below drag-divergence Mach number.

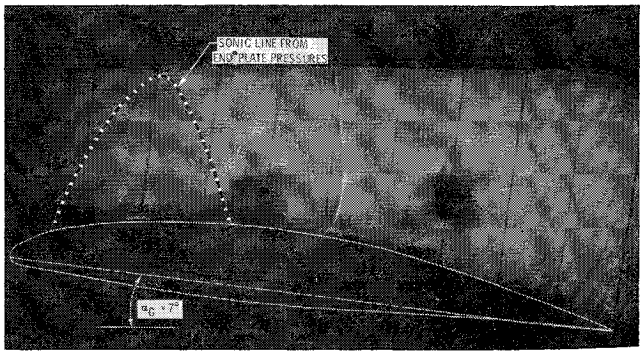

Fig. 11b Spark shadowgraph above drag-divergence Mach number.

airfoil. These plots indicate a smooth fairing at the front of the airfoil, but at the downstream end of the isobars there is considerable discontinuity. This set of pressure data was used to obtain the sonic lines superimposed on the shadowgraphs of Figs. 11a and 11b.

The end plate sonic line position in Fig. 11b shows that, when there is appreciable shock wave interaction with the boundary layers on the end plates and the airfoil, there is a definite degradation of the flow two-dimensionality. Some flow visualization studies of the model surface conditions showed that there was corner separation where the end plates join the airfoil. However, this occurred over a small fraction of the test span and seemed to cause little trouble in determining the drag divergence boundary. The major effect was degradation of the end plate pressure measurements due to the end plate boundary layer, but the shock wave shadowgraphs accurately showed the field flow conditions corresponding to the centerline surface pressure measurements.

Effect of End Plate Size

Tests to date have indicated that extensive regions of supersonic flow with local Mach numbers up to 1.5 can be obtained over the upper surface of an airfoil. These supersonic flow regions extend almost to the top of the upper half of the end plate. The present end plate size will probably limit the maximum local Mach number that can be obtained

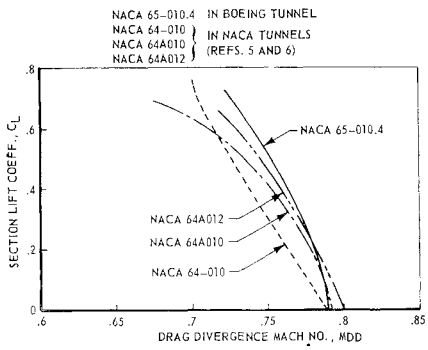

Fig. 12a Comparison of drag-divergence boundaries with NACA data.

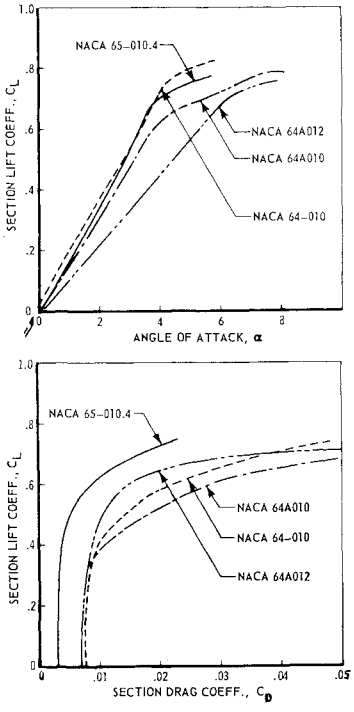

Fig. 12b Comparison of lift and drag with NACA data at Mach 0.75.

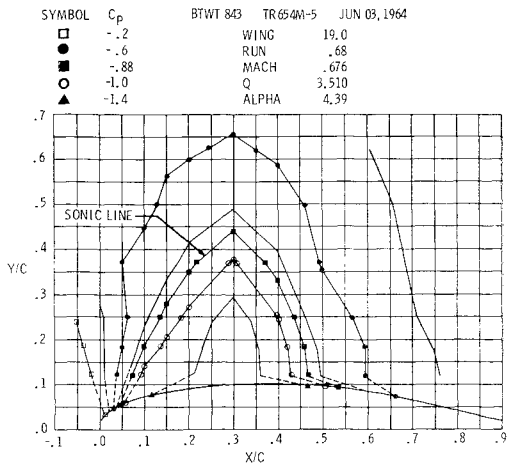

Fig. 13a End plate and centerline surface pressure correlation, below drag-divergence Mach number.

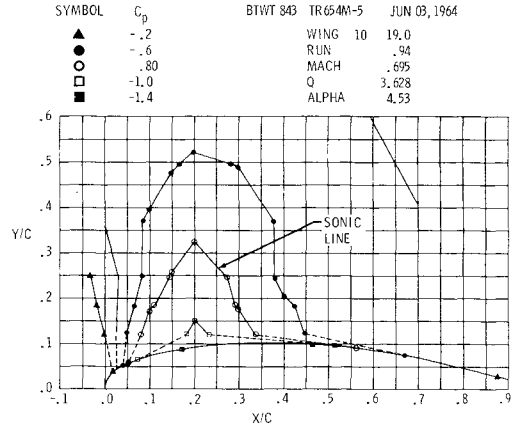

Fig. 13b End plate and centerline surface pressure correlation, above drag-divergence Mach number.

over the airfoil while maintaining reasonable approximation to two-dimensional flow conditions. To check this, an end plate of twice the height has been tested. It was found that, although there was a substantial change in the effective aspect ratio of the model appropriate to the difference in end plate size, the character of the aerodynamic results did not otherwise change. This would indicate that the end plate diameter of two chords is adequate for testing airfoils well into the drag rise.

Associated with the size of the end plate is the end plate boundary layer. The separation properties of the 40-in. end plate boundary layer have been marginally satisfactory to date. For future wing sections, having higher lift and Mach capability, separation of the end plate boundary layer may be a limiting factor. Therefore, end plate blowing boundary-layer control will be investigated to determine the extent of interference imposed by such separation effects.

There are no corrections applied to the test data for blockage or wind-tunnel wall effects. Actually, the single wall slot in the immediate vicinity of the model provides an unknown high-speed flow environment for this installation. However, based on tests of 707 wing sections that correlated fairly well with known free-flight results and the NACA data correlations just discussed, the configuration provides sufficient pressure relief to eliminate the need for such corrections.

Another limitation may occur when the pressure gradients imposed on the tunnel floor boundary layer are sufficient to cause local flow choking below the lower end plate. It also could cause excessive upflow at the leading edge of the lower end plate and result in a flow separation. Again, it may be necessary to enforce some methods of control over this flow

condition at higher Mach number, if it becomes a significant problem.

Performance of the Wake Rake

The wake rake shown in Fig. 5 has an upper row of static-pressure tubes in the "biplane" structure and a lower row of total-pressure tubes. The large tube at the support end of the total-pressure array is a yaw head. The formula used to compute the drag from the wake measurement is based on the Betz formula modified for compressibility. The measuring station is 30% of the chord downstream from the trailing edge. This position was chosen as a reasonable compromise between the lateral spread of the wake profile and the value of the peak total-pressure loss. At this station, the static-pressure measurements correct the value of computed drag by 2–4% as compared with the results obtained by assuming that the pressure at this point is freestream static.

Conclusions

The technique described for testing airfoil sections at transonic speeds offers the following advantages over that used previously at Boeing: 1) the large models can be constructed more accurately, permitting more sophisticated variations in airfoil design and test techniques, 2) the Reynolds number is significantly closer to fullscale conditions, 3) sidewall boundary-layer effects are minimized, 4) on-line analog data permit continuous monitoring and control of the test program to optimize tunnel utilization, 5) conversion of the tunnel to the transonic airfoil testing configuration is minimal, and 6) electronic data processing and plotting provide overnight availability of the final results.

It has been possible to obtain accurate data well into the drag rise and buffet regions of airfoil operation. However, this testing technique possesses limitations to the maximum test Mach numbers and flow conditions that have satisfactory two-dimensional flow in the airfoil test region.

References

[1] Wimpress, J. K. and Swihart, J. M., "Influences of aerodynamic research on the performance of supersonic airplanes," J. Aircraft **1**, 71–76 (1964).

[2] Pearcey, H. H., "The aerodynamic design of section shapes for swept wings," *Advances in Aeronautical Sciences* (Pergamon Press, New York, 1962), Vol. 3, p. 277.

[3] Stratford, B. S., "The prediction of separation of the turbulent boundary layer," J. Fluid Mech. **5**, 1–16 (1959) pp. 1–16.

[4] Holder, D. W., "The transonic flow past two-dimensional aerofoils," J. Roy. Aeronaut. Soc. **68**, 501–516 (1964).

[5] *S-C 4020 High-Speed Microfilm Recorder Programming Manual* (Department PM-1 General Dynamics/Electronics, San Diego, Calif., July 1961).

[6] Hemenover, A. D., "Tests of NACA 64-010 and 64A010 airfoil sections at high subsonic Mach numbers," NACA Research Memo. A9E31 (July 8, 1949).

[7] Daly, B. N. and Dick, R. S., "Effect of thickness camber, and thickness distribution on airfoil characteristics at Mach numbers up to 1.0," NACA TN 3607 (March 1956).